Designation: D8093 – 16

An American National Standard

Standard Guide for Nondestructive Evaluation of Nuclear Grade Graphite[1]

This standard is issued under the fixed designation D8093; the number immediately following the designation indicates the year of original adoption or, in the case of revision, the year of last revision. A number in parentheses indicates the year of last reapproval. A superscript epsilon (ε) indicates an editorial change since the last revision or reapproval.

1. Scope

1.1 This guide provides general tutorial information regarding the application of conventional nondestructive evaluation technologies (NDE) to nuclear grade graphite. An introduction will be provided to the characteristics of graphite that defines the inspection technologies that can be applied and the limitations imposed by the microstructure. This guide does not provide specific techniques or acceptance criteria for end-user examinations but is intended to provide information that will assist in identifying and developing suitable approaches.

1.2 The values stated in SI units are to be regarded as the standard.

1.2.1 *Exception*—Alternative units provided in parentheses are for information only.

1.3 *This standard does not purport to address all of the safety concerns, if any, associated with its use. It is the responsibility of the user of this standard to establish appropriate safety and health practices and determine the applicability of regulatory limitations prior to use.*

2. Referenced Documents

2.1 *ASTM Standards:*[2]

C709 Terminology Relating to Manufactured Carbon and Graphite

D7219 Specification for Isotropic and Near-isotropic Nuclear Graphites

E94 Guide for Radiographic Examination

E1025 Practice for Design, Manufacture, and Material Grouping Classification of Hole-Type Image Quality Indicators (IQI) Used for Radiology

E1441 Guide for Computed Tomography (CT) Imaging

3. Summary of Guide

3.1 This guide describes the impact specific material properties have on the application of three nondestructive evaluation technologies: Eddy current/electromagentic testing (ET) (surface/near surface interrogation), ultrasonic testing (UT) (volumetric interrogation), radiographic (X-ray) testing (RT) (volumetric interrogation), to nuclear grade graphite.

4. Significance and Use

4.1 Nuclear grade graphite is a composite material made from petroleum or a coal-tar-based coke and a pitch binder. Manufacturing graphite is an iterative process of baking and pitch impregnation of a formed billet prior to final graphitization, which occurs at temperatures greater than 2500 °C. The impregnation and rebake step is repeated several times until the desired product density is obtained. Integral to this process is the use of isotropic cokes and a forming process (that is, isostatically molded, vibrationally molded, or extruded) that is intended to obtain an isotropic or near isotropic material. However, the source, size, and blend of the starting materials as well as the forming process of the green billet will impart unique material properties as well as variations within the final product. There will be density variations from the billet surface inward and different physical properties with and transverse the grain direction. Material variations are expected within individual billets as well as billet-to-billet and lot-to-lot. Other manufacturing defects of interest include large pores, inclusions, and cracks. In addition to the material variation inherent to the manufacturing process, graphite will experience changes in volume, mechanical strength, and thermal properties while in service in a nuclear reactor along with the possibility of cracking due to stress and oxidation resulting from constituents in the gas coolant or oxygen ingress. Therefore, there is the recognized need to be able to nondestructively characterize a variety of material attributes such as uniformity, isotropy, and porosity distributions as a means to assure consistent stock material. This need also includes the ability to detect isolated defects such as cracks, large pores and inclusions, or distributed material damage such as material loss due to oxidation. The use of this guide is to acquire a basic understanding of the unique attributes of nuclear grade graphite

[1] This guide is under the jurisdiction of ASTM Committee D02 on Petroleum Products, Liquid Fuels, and Lubricants and is the direct responsibility of Subcommittee D02.F0 on Manufactured Carbon and Graphite Products.

Current edition approved Dec. 1, 2016. Published March 2017. DOI: 10.1520/D8093-16.

[2] For referenced ASTM standards, visit the ASTM website, www.astm.org, or contact ASTM Customer Service at service@astm.org. For *Annual Book of ASTM Standards* volume information, refer to the standard's Document Summary page on the ASTM website.

and its application that either permits or hinders the use of conventional eddy current, ultrasonic, or X-ray inspection technologies.

5. Graphite Properties

5.1 Table 1 provides a summary of pertinent material properties for a limited selection of commercial nuclear graphite types.

5.2 The composite nature of graphite results in a multipart microstructure with variably shaped and sized porosity (see Fig. 1). The innate porosity in essence forms a flaw population that, in part, dictates not only material properties, but the minimum size limit of isolated flaws that conventional NDE technologies can and or should differentiate. However, this is not to overlook the potential need to detect and characterize distributed flaw populations such as oxidation or radiation damage that may be dimensionally smaller than the inherent porosity. The nature of the microstructure along with the material properties of low electrical conductivity, low acoustic velocity, and limited material constituents will dictate how the various NDE technologies can be applied and limit the information available from the examinations.

6. Eddy Current Examinations

6.1 Eddy current testing (ET) is an established inspection technology well suited for surface/near surface inspection of electrically conductive components. ET is based on generating eddy currents in an electrically conductive test sample through inductive coupling with a test coil. The characteristics and depth of the interrogating eddy currents are governed by the bulk electromagnetic properties of the test piece, test piece geometry, test frequency, and degree of electromagnetic coupling. The primary electromagnetic properties of interest are electrical conductivity and magnetic permeability. Any material or physical condition (for example, cracks, porosity, changes in grain structure, or different phases) that locally affects one or both of these properties can be detected and characterized. Typically, material anomalies are sensed through changes in the drive coil impedance when coupled to the test piece but can also be detected by means of secondary pickup induction coils or other magnetic field measurement technologies, for example, Hall or giant magnetoresistive (GMR) devices. The approaches and test probes that can be implemented are diverse and dependent on the type, size, and location of the material anomaly or condition of interest as well as the test piece electromagnetic properties, geometry, surface condition, microstructure, temperature, and so forth.

6.2 Eddy currents can be used to inspect nuclear graphite for the presence of surface/near surface cracks, voids, and inclusions as well as to characterize the distribution of porosity or other distributed flaw populations that affect the bulk electrical conductivity. Aspects to consider when applying eddy currents to nuclear graphite include its low electrical conductivity, microstructure, and test conditions. The measured electrical conductivity of nuclear graphite is in the range of 0.1×10^6 to 0.9×10^6 S/m, making it less than or nearly equal in conductivity to low conductivity metal alloys such as Ti-6Al-4V titanium (0.58×10^6 S/m), Inconel 600 (1.02×10^6 S/m), and stainless steel 304 (1.39×10^6 S/m) (**1**).[3] For low conductivity materials such as this, the dominance of skin effect (the exponential decay of eddy current density in test sample) will be significantly reduced compared to that of probe coil diameter to control depth sensitivity. The plane-wave approximation of eddy current density, j_x, in a test piece yields Eq 1 (**2**):

$$j_x = j_0 e^{\left(-x\sqrt{(\pi f \mu \sigma)}\right)} \quad (1)$$

where:

j_x = current density in test piece at depth x (A/m^2),
j_0 = current density at test piece surface (A/m^2),
x = depth into test piece (m),
π = 3.1416,
f = test frequency (Hz),
μ = magnetic permeability in free space ($4\pi \times 10^{-7}$ H/m), and
σ = test piece electrical conductivity (S/m).

6.3 The standard depth of penetration, $\delta = 1/\sqrt{(\pi f \mu \sigma)}$, is defined as the depth at which the eddy current density drops to 1/e or 36.8 % of the value of j_0. Although eddy currents will be generated past 1δ, they attenuate rapidly. Eddy current density at 2δ is only 13.5 % of j_0. It should also be noted that the phase of the eddy currents progressively lags with depth into the test

[3] The boldface numbers in parentheses refer to a list of references at the end of this standard.

TABLE 1 Graphite Properties[A]

Graphite Designation/ Manufacturer	Density (kg/m^3)		Electrical Resistivity (μΩ-m)		L-Wave Acoustic Velocity (km/s)		S-Wave Acoustic Velocity (km/s)		Maximum Average Particle (Grain) Size (mm)	Forming Process
	WG	AG	WG	AG	WG	AG	WG	AG		
PCEA/ GrafTech International	1.775e+003	1.781e+003	7.49	8.01	2.65	2.56	1.59	1.58	0.7	Extruded
NBG-17/ SGL Group	1.850e+003	1.843e+003	9.51	9.84	2.77	2.76	1.61	1.61	0.8	Vibrationally molded
NBG-18/ SGL Group	1.871e+003	1.872e+003	9.57	9.16	2.87	2.93	1.67	1.68	1.6	Vibrationally molded
IG-110/ Toyo Tanso USA Inc.	1.777e+003	1.778e+003	11.24	10.98	2.46	2.51	1.56	1.57	0.01	Isostatically molded
IG-430/ Toyo Tanso USA Inc.	1.812e+003	1.814e+003	9.78	8.62	2.40	2.57	1.54	1.58	0.01	Isostatically molded

[A] Idaho National Laboratory AGC 2 sample measurements: Average values for small, evenly distributed samples sectioned from a single billet, against grain (AG) and with grain (WG) directions are determined by orientation of the primary sample axis when sectioned from billet.

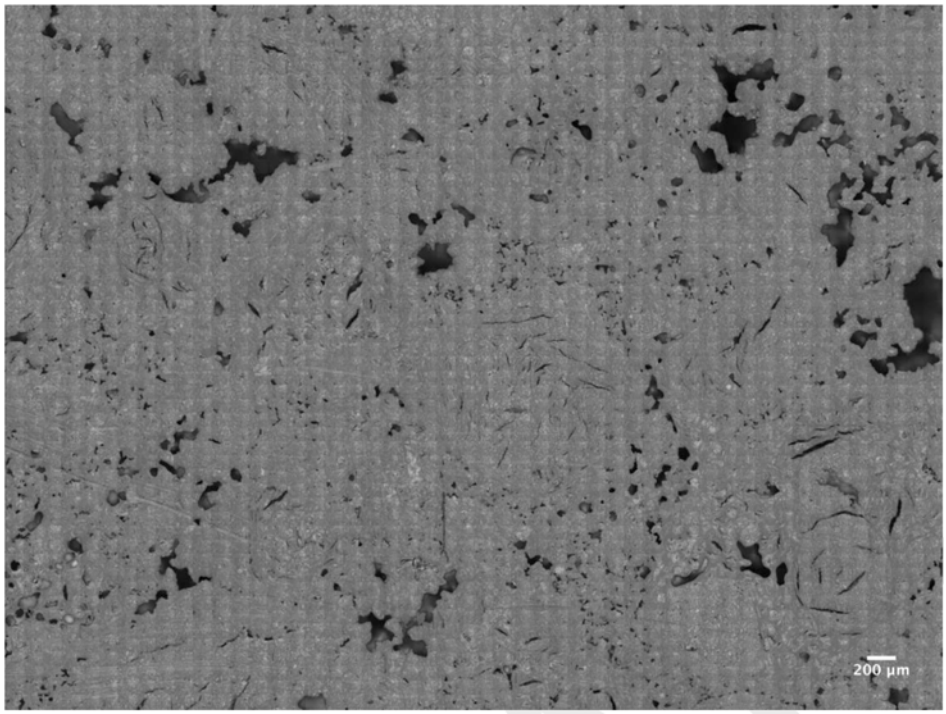

FIG. 1 Micrograph of SGL Group, NBG-18 Graphite

piece which is used to differentiate the source of the signal. Each standard depth produces 1 radian (57.3°) of phase lag. High current density yields good detectability and the standard depth of penetration is typically adjusted by means of manipulation of the test frequency to optimize current density and signal phase for defect detection or the measurement of interest. For example, selecting a test frequency that yields a 1δ at the depth where defects are expected to be located for a specific test piece should provide sufficient current density (approximately 37 % of surface current density) to detect defects at that depth and provide an approximate defect signal phase shift of 115° compared to a surface lift-off response (**2**). Lift-off is the response obtained from decoupling of the probe coil from the test piece due to increased probe coil to test piece separation or surface roughness, and higher test frequencies are required to get an equivalent δ for graphite compared to a metal. To get a $\delta = 0.005$ m in SS304 ($\sigma = 1.39 \times 10^6$ S⁄m), a test frequency of approximately 7.3 kHz is required. For graphite with a conductivity of 0.5×10^6 S⁄m, a test frequency of approximately 20.3 kHz is required. However, to obtain adequate eddy current density at the calculated skin depth, the induction probe coil must be able to project a sufficiently strong magnetic field to that depth.

6.4 A factor determining depth of penetration of the magnetic field into the test piece and thus the production of eddy currents will be the extent and magnitude of the axial field projected by a probe coil. The extent of the axial field projection is directly proportional to the diameter of the coil windings with a magnitude that decreases rapidly down the axis away from the coil. At an axial distance equal to ⅓ the coil diameter the field strength is approximately 50 % of the field strength at the coil face, and at a distance equal to 1 diameter only 10 % of the field strength remains (**2**). Compared to high conductivity metals, the projection limit of the axial field of the test coil may control the depth sensitivity in graphite versus skin depth. Therefore, proper selection of probe coil size combined with suitable low test frequencies will permit much thicker sections of graphite to be interrogated compared to an equivalent probe coil and a high conductivity metal combination. This provides the capability to perform limited volumetric examinations to detect large internal defects or characterize variations in bulk microstructural features such as porosity. Note that the area interrogated by the probe coil is proportional to its size and orientation. To improve detection of smaller surface defects, that is, concentrate eddy currents near the surface in a confined space, high test frequencies and smaller probe coils should be implemented (see Fig. 2). However, the coarse microstructure of some graphite types may introduce significant material noise. In this case, the 0.8 mm diameter by 0.8 mm deep flat bottom hole is equivalent in size to surface breaking porosity inherent to the graphite.

6.5 Per Specification D7219 and Terminology C709, grain sizes of the starting material in the mix for nuclear graphite can range from a maximum of 1.68 mm (medium grained) down to less than 2 micron (microfine grained). The size of the resulting microstructural features within the graphite (“grains” and porosity) will also range in a similar manner, as will the material noise recorded during inspections. That will limit the size of an anomaly or material variation that can be detected to something larger than the inherent microstructure. Medium grain materials will produce significantly more material noise than a fine grain material (see Fig. 3). This is especially true for the examination of machined surfaces using smaller diameter probes at high test frequencies. The rough, as-manufactured

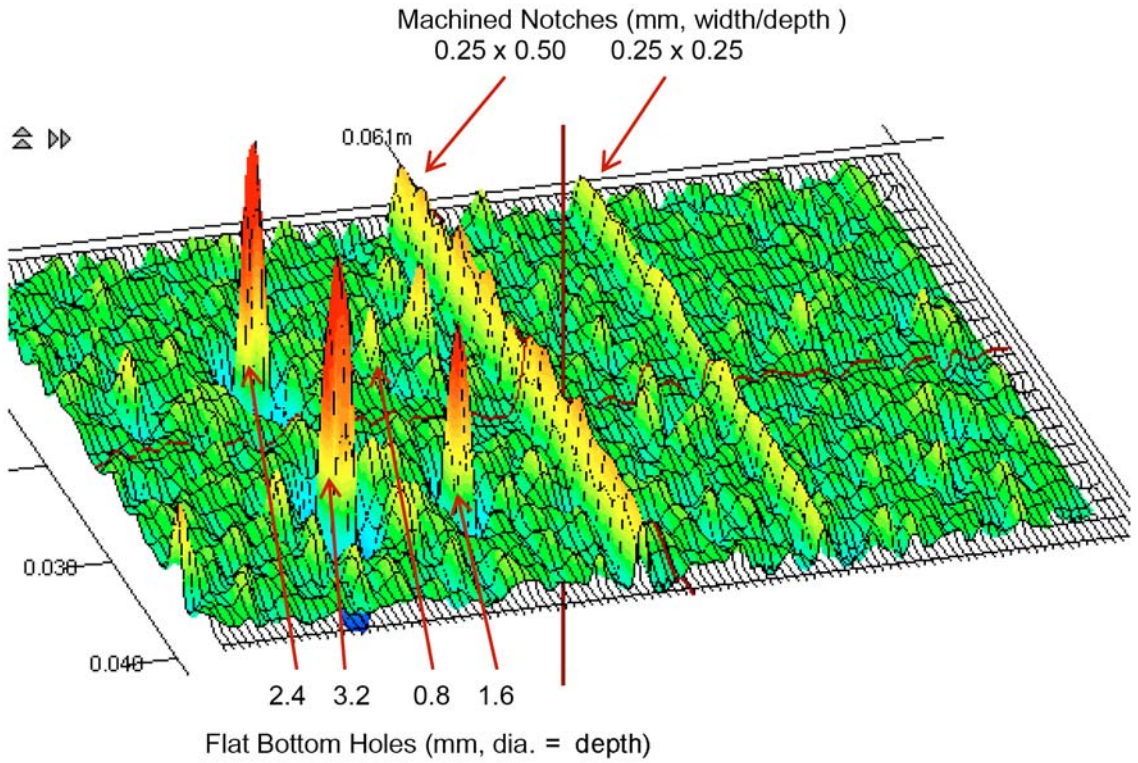

The data was collected at 500 kHz using a 64 element transmit-receive array probe (2.0 mm coils separated by 2.5 mm, array element pitch is 1.25 mm). Although detectable, the 0.8 mm diameter by 0.8 mm deep flat bottom hole produces signals equivalent to the surface breaking porosity inherent to the graphite.

FIG. 2 Eddy Current Scan of NBG-18 Graphite Containing Artificial Flaws

surface of a billet will present a similar problem. The workmanship, finish, and appearance criteria in Specification D7219 only require a billet to be brushed clean after removal from the graphitization furnace resulting in rough, potentially uneven surfaces that will introduce significant material and lift-off noise into the signal. In both cases, probe diameter, design, test frequencies, or filtering can be adjusted to help mitigate the noise, assuming the defect or material anomaly of interest is of a nature to provide a relevant indication.

7. Ultrasonic Examinations

7.1 Ultrasonic inspection is based on the interaction of an acoustic wave with the material through which it is propagating. Isolated, macroscopic discontinuities are typically detected by means of their interaction with the acoustic wave to produce a reflection (echo) that propagates back to the transmitting transducer or a secondary pickup transducer. The nature of the interaction is in part defined by the mismatch of the acoustic impedance between the discontinuity and the matrix as well as the size of the discontinuity versus the ultrasonic wavelength. The acoustic impedance of a material is the product of its density and acoustic velocity and as the impedance mismatch at the boundary of a discontinuity increases, so does the amount of energy that is reflected.

7.1.1 Wavelength plays a role in that discontinuities equal to or larger than the wavelength will strongly interact with the passing wave, while those smaller than the acoustic wavelength will have little interaction. As a result, test frequencies are typically selected to provide wavelengths smaller than the defects of interest. At a specific acoustic velocity, an increase in test frequency will decrease the wavelength size. However, the characteristic microstructure of graphite tends to strongly attenuate high test frequencies, reducing waveform penetration into the graphite as well as limiting the size of defect that can be detected. An example of the high frequency attenuation that can be expected for a medium grain graphite is provided in Fig. 4. The transducer used for this example yielded a center frequency of 2.2 MHz for the first back wall reflection recorded from a 9.75 mm thick fused silica optical flat. Note that for the NBG-18, a test frequency of less than 1 MHz will be required to permit significant material penetration without excessive signal attenuation.

7.1.2 The acoustic velocity of NBG-18 is 2.9 km⁄s which yields a 5.8 mm wavelength at 0.5 MHz. As a rule of thumb, detection of isolated discontinuities with dimension of approximately one-half the ultrasonic wavelength is viable. Presented in Fig. 5 is a B-scan image from a 93.9 mm thick test block of NBG-18 graphite containing 3 mm diameter side-drilled holes ranging from 10 mm to 70 mm in depth from the surface. The B-scan data was collected using a 25.4 mm diameter, 0.5 MHz contact transducer with water coupling. The top and bottom surface of the test block was machined to provide uniform thickness and coupling. Note that a microstructural anomaly in the region of the 40 mm side-drilled hole significantly reduced

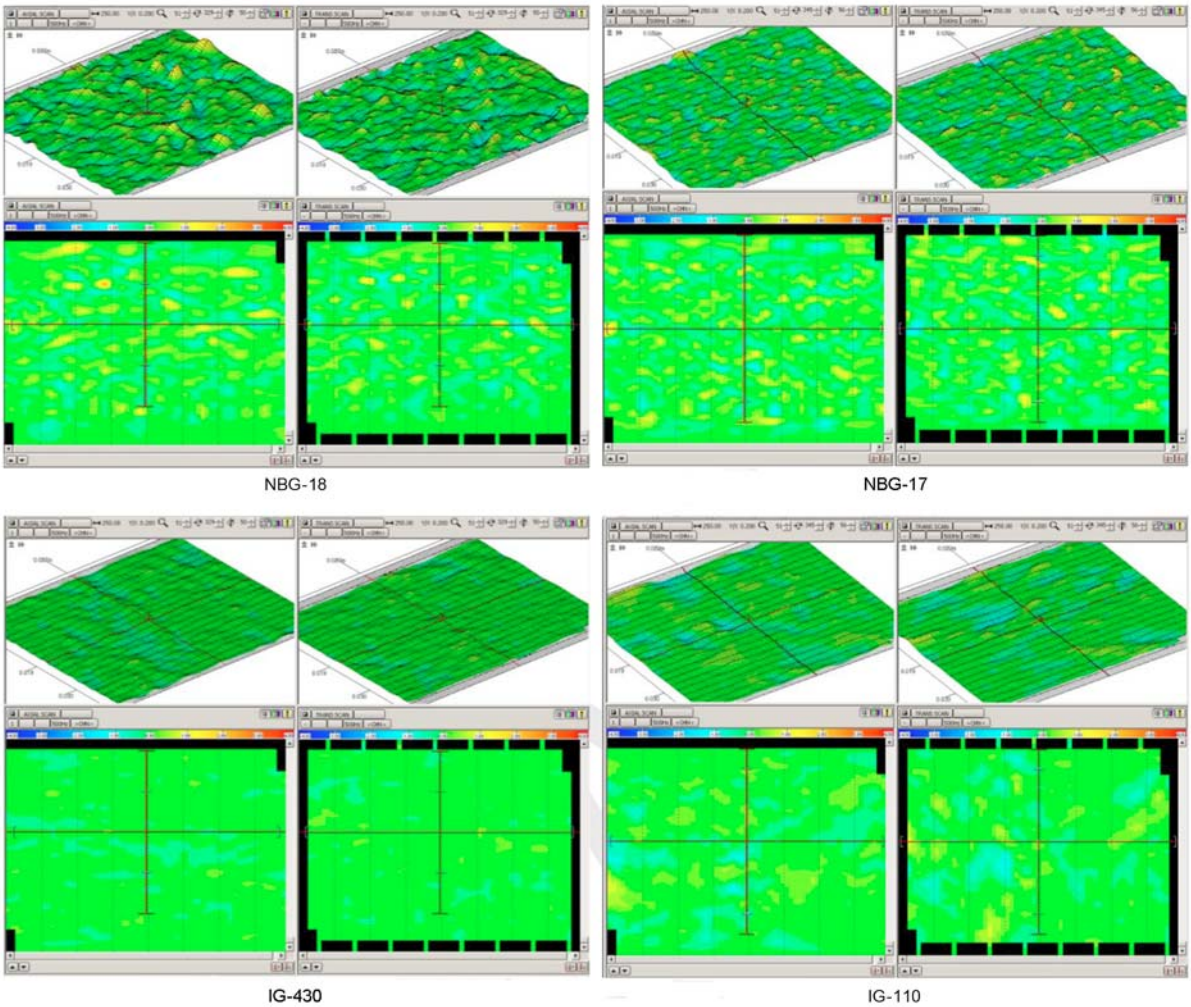

The approximate dimensions of each C-scan is 40 mm by 40 mm. The data was collected at 500 kHz using a 64 element transmit-receive array probe (2.0 mm coils separated by 2.5 mm, array element pitch is 1.25 mm). Two C-scans are obtained during a single scan. The transverse C-scan is primarily sensitive to transverse-oriented defects while the axial C-scan is sensitive to axial-oriented defects.

FIG. 3 Eddy Current C-Scans Comparing the Material Noise Obtained from Medium Grain (NBG-18, 1.6 mm and NBG-17, 0.8 mm Grain Size) Versus Superfine Grain (IG-430 and IG-110, 10 µm Grain Size) Nuclear Graphites

the signal-to-noise ratio for this indication. Using instrumentation or techniques that increase the acoustic energy introduced into the material, for example, high energy narrowband techniques, will help to improve acoustic wave penetration and signal-to-noise ratios for material anomalies. Finer grain graphite will suffer less but still have significant attenuation. Overall, the material variations often observed in graphite will reduce depth and sizing accuracy.

7.1.3 Fig. 6 compares ultrasonic back wall echoes from the 93.9 mm thick NBG-18 graphite (1.6 mm grain size) test block to those from an 88.8 mm thick IG-110 graphite (10 µm grain size) test block. The A-scans were collected using the same instrument settings and the same 25.4 mm diameter, 2.25 MHz transducer used in Fig. 4. Although the superfine grain IG-110 graphite suffers less attenuation, the center frequency of the back wall reflection still drops to approximately 1 MHz (waveform and FFT bottom of Fig. 6) from the 2.25 MHz center frequency of the input signal and has a highly attenuated second back wall reflection.

7.1.4 Ultrasonics can also be used to perform material characterization or detect distributed flaw populations by means of measurement of various wave propagation properties such as velocity, attenuation, or scattering. Elastic interactions as defined by the elastic constants influence acoustic velocity which can also be modified by acoustic energy scattered from the microstructure. Anelastic interactions result in loss of propagating wave energy by mechanisms that produce heat or transformation into different forms of sound. Of the three properties, velocity measurements will be the most viable approach to acquiring information regarding material uniformity (microstructure and porosity), isotropy, or the presence of distributed flaw populations. Fig. 7 compares time-of-flight C-scans from sections of machined NBG-17 and NBG-18 test blocks. The data was collected using a 25.4 mm, 0.5 MHz contact transducer with water couplant. The values presented are the round trip time-of-flight to the maximum negative peak amplitude of the back wall reflection. Neglecting possible variations in thickness due to tolerances in machining, the

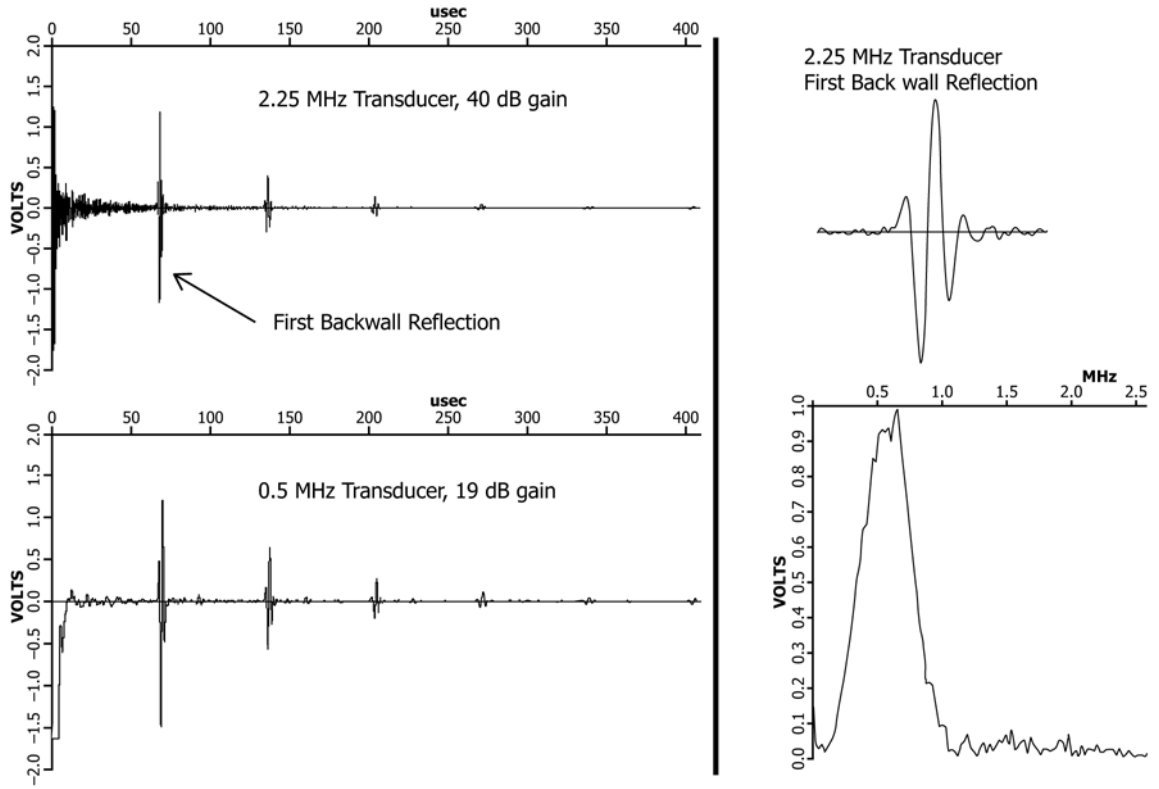

A square wave pulser-receiver was used with 25.4 mm diameter, 2.25 MHz, and 0.5 MHz contact transducers with water couplant. Pulse width was set using fixed instrument settings, and no frequency filters were engaged. (*a*): Complete A-scans with multiple backwall reflections. (*b*): First backwall reflection using 2.25 MHz transducer and corresponding waveform FFT. The 0.6 MHz center frequency of the reflection indicates significant attenuation of the high frequency content in the propagating wave.

FIG. 4 Ultrasonic Pulse-Echo A-Scans, Collected at One Location from a 93.9 mm Thick Machined NBG-18 Graphite Plate

0.406 m thick NBG-18 test block had a 5 µs range in time-of-flight values compared to 1 µs range of the 0.467 m thick NBG-17 test block. These ultrasonic scans illustrate that the variation in acoustic velocity provides a measure of the uniformity of the microstructure and therefore the uniformity of the mechanical properties within each test piece.

7.1.5 The prior examples all used contact transducers with water coupling. Requirements to prevent contamination of the graphite may prevent the use of liquid coupling. Alternative technologies include dry contact roller probes, laser-based generation and detection, air-coupled transducers, and electromagnetic-based transducers. However, compared to liquid-coupled piezoelectric transducers, the efficiency of ultrasonic wave generation and detection in the test piece for these approaches are reduced. For comparison, the response for a 0.5 MHz liquid-coupled transducer to an equivalent simulated dry contact roller probe is provided in Fig. 8. Transducer and instrument settings were the same for the two measurements. Although demonstrated to be a viable approach to ultrasonic coupling into graphite, a significant reduction in signal amplitude and quality is observed for the simulated roller probe. The loss of signal amplitude and quality will reduce measurement reliability and defect detection capabilities. Also note that a transmit-receive arrangement for a roller probe would help to remove the signal interference introduced by the probe structure and test piece front surface at the depth of the side-drilled hole.

7.2 Noncontacting laser-based, air-coupled, or electromagnetically coupled ultrasonic approaches will eliminate the potential for material contamination by means of surface contact. Combinations of the different approaches, for example, laser generation with EMAT detection, have also been investigated (**3**). Although applicable, these approaches also have limitations with respect to sensitivity and their application to graphite.

7.3 Air-coupled ultrasound has been utilized for material interrogation primarily to detect defects in low-impedance solids such as foams, plastics, and composite materials. The challenge in using air-coupled ultrasound for solid materials is the large impedance mismatch between the air and the material that results in low energy transmission into the material. A similar loss of energy will occur at the transducer-air interface without impedance matching. The reflection coefficient, *R*, for a normal incidence acoustic wave is (**4**):

$$Rp = (Z_2 - Z_1) / (Z_1 + Z_2) \quad (2)$$

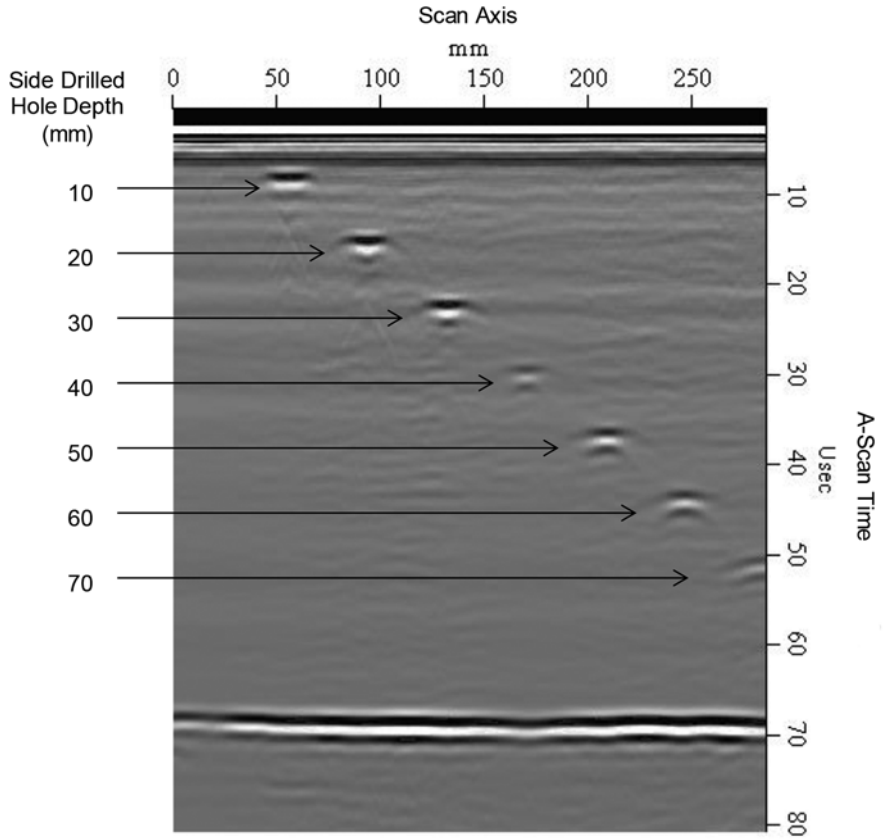

The data was collected using a 25.4 mm diameter, 0.5 MHz contact transducer with water couplant. Note that the back wall echo varied in both amplitude and time, indicating material conditions exist within the test sample that alter signal attenuation and velocity. This will reduce defect depth and sizing accuracy.

FIG. 5 B-Scan Image of NBG-18 Test Block Containing 3 mm Diameter Side-Drilled Holes

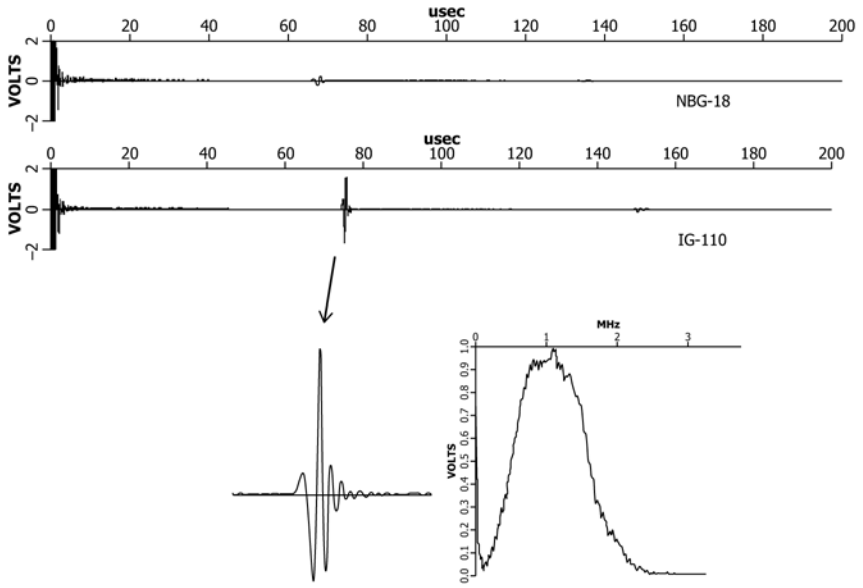

As demonstrated by the recorded waveform and FFT, the IG-110 does not attenuate the amplitude or higher frequencies as much as the coarser grain NBG-18.

FIG. 6 Ultrasonic A-Scans Comparing Ultrasonic Wave Attenuation for a Medium Grain NBG-18 (1.6 mm Grain Size) Graphite to a Superfine IG-110 (10 µm Grain Size) Graphite

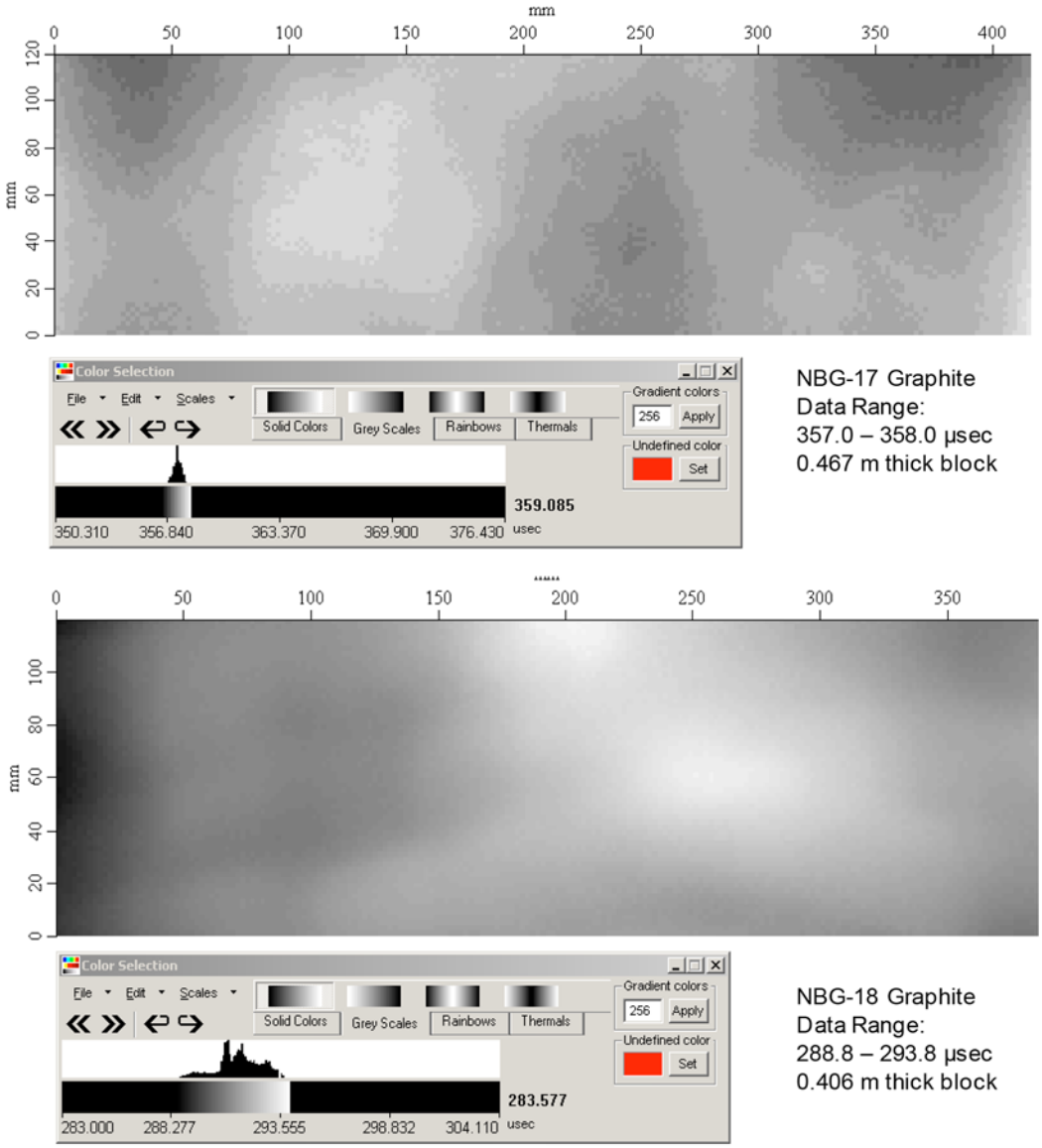

Acquired using a 25.4 mm diameter, 0.5 MHz contact transducer with water couplant. The time-of-flight values presented are the round trip times to the maximum negative peak of the back wall reflection.

FIG. 7 Time-of-Flight C-Scans of NBG-17 and NBG-18 Machined Test Blocks

where:

Rp = reflection coefficient based on acoustic pressure ratios,
Z_n = $\rho_n c_n$ = acoustic impedance (kg/m^2-s),
c_n = acoustic velocity of material n (m/s), and
ρ_n = density of material n (kg/m^3).

7.3.1 At an air- (Z = 0.0004 x 10^6 kg/m^2-s) (**3**) graphite (Z ≈ 4.7 x 10^6 kg/m^2-s) interface, the reflection coefficient is approximately 0.99, indicating almost complete reflection of the acoustic wave. To overcome these issues, sensitive-low noise instrumentation is combined with optimized transducers and drive signals to produce high sound pressures, for example, using high voltage drives, air impedance matching, and tone bursts with resonant elements. In addition, digital filters and signal processing approaches have been implemented to significantly improve the signal-to-noise ratio for the low amplitude responses. Another factor affecting air-coupled ultrasonics is that sound is strongly attenuated above 1 MHz in air. This characteristic limits most applications to test frequencies less than 1 MHz which does match with the test frequencies practical for thick graphite sections. With an optimized system and careful alignment, air-coupled ultrasonics can be used to perform basic ultrasonic measurements such as velocity or detect relatively large defects (see Fig. 9).

7.4 Laser ultrasonics is a noncontact approach to generate and detect ultrasonic waves in materials. While laser-coupled ultrasound does not require physical contact, it does involve converting between mechanical and optical energy. It is principally limited by the amount of ultrasonic energy that can be produced in the sample and the amount of ultrasonic energy required for detection. A short laser pulse (femto to nanosecond

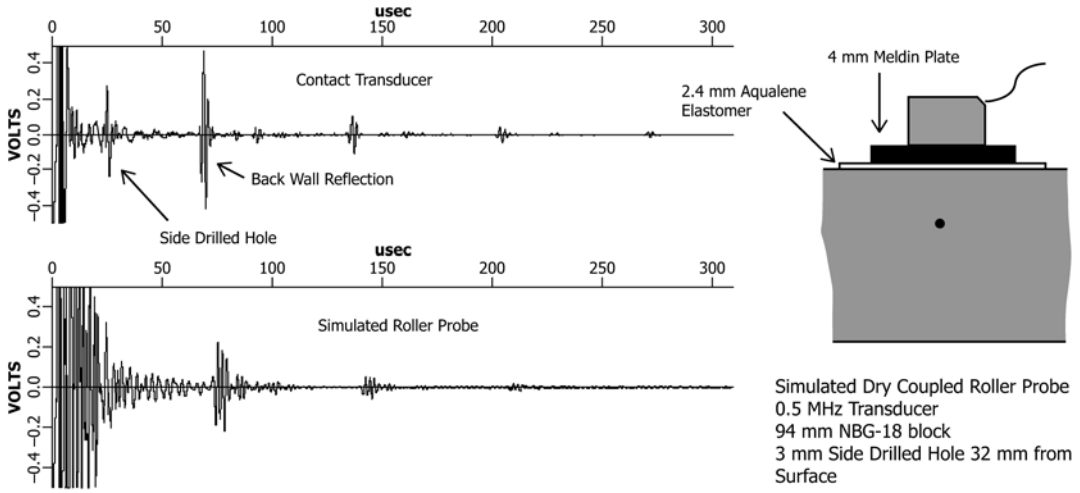

FIG. 8 A-Scan Comparison for 0.5 MHz Water-Coupled Contact Transducer to a Simulated 0.5 MHz Dry-Coupled Roller Probe

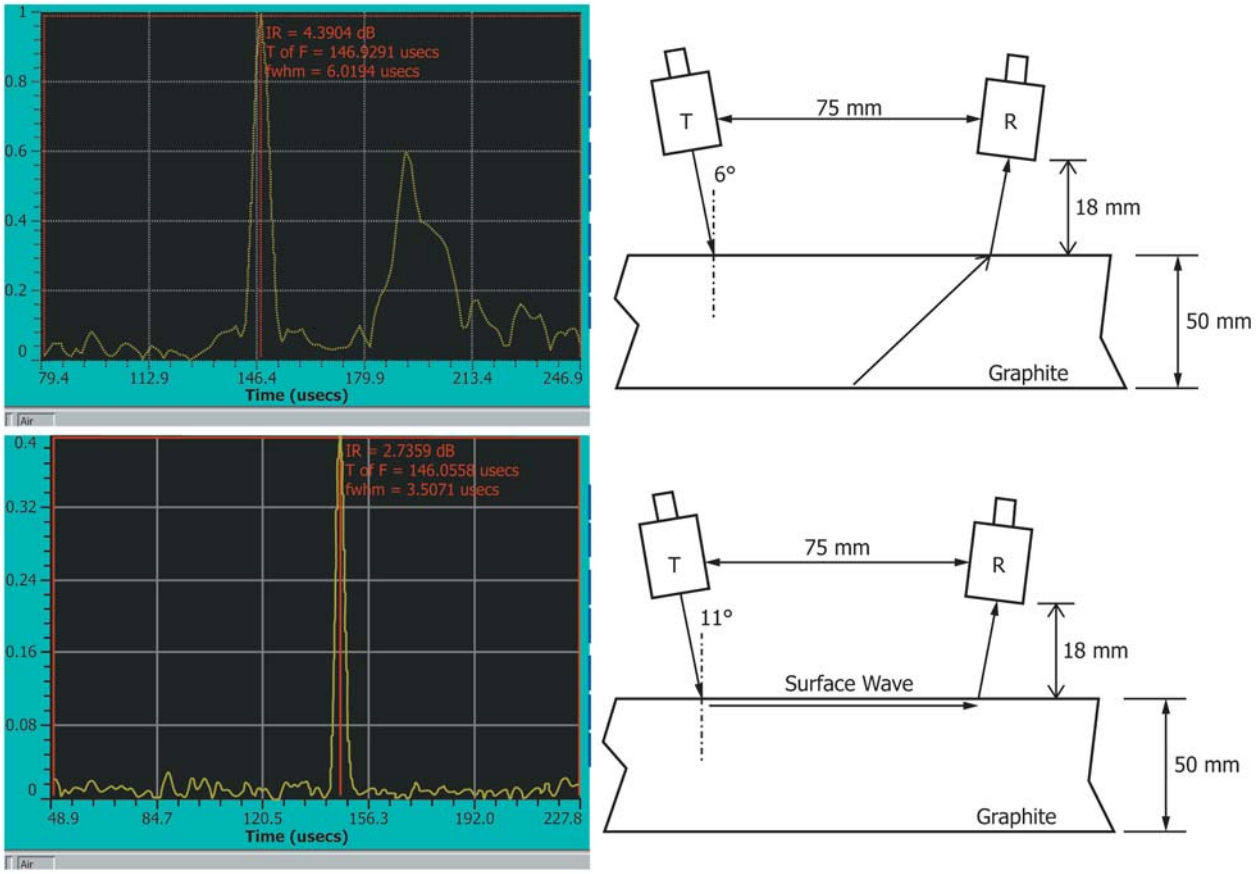

Data was collected using a Second Wave NCA-1000 system with NCT-55, 0.5 MHz, 12.5 mm diameter transducers.

FIG. 9 Air-Coupled Ultrasound Responses from a 50 mm Thick Graphite Sample

time periods) is used to generate acoustic waves by means of thermoelastic expansion or ablation. In the thermoelastic regime, the short laser pulse produces a rapid thermal expansion on the material surface that produces bulk and surface acoustic waves. In the ablation regime, sufficient energy is used to expel material from the sample surface, resulting in a recoil effect that produces the acoustic waves. Frequently, a plasma is also generated that contributes to acoustic generation. The different mechanism of acoustic wave generation will produce different acoustic modes and wave directivity. The frequency content of the generated ultrasound is determined by pulse duration, surface spot size, and mode of generation but is typically high when compared to the test frequencies suitable for graphite. Acoustic wave detection is accomplished using a

second laser and a detector based on various techniques, for example, interferometry or beam deflection. The technique used will depend on the characteristics of the test material and its surface condition, mirror versus diffuse. Sufficient light from the detection laser needs to be reflected from the surface to permit the detection technique to function. Unlike metals, graphite does not efficiently reflect light even when polished and therefore presents a challenge for laser-based detection of ultrasonic signals.

7.5 Laser ultrasonics is applicable to graphite but as explained before, the unique characteristics of graphite results in a different behavior when compared to a metal (see Fig. 10). The laser ultrasonic response of an isotropic metal, for example, aluminum, is well defined and can be easily modeled while the response from the medium grain NBG-18 sample demonstrates viscoelastic behavior. While ultrafine grain IG-110 shows less viscoelastic behavior, it still does not respond as cleanly as a metal.

7.6 The ablation threshold for graphite is also different than a metal. As compared to aluminum, which demonstrates an ablation threshold of approximately 5 MW/cm^2, NBG-18 graphite yields a threshold of roughly 14 MW/cm^2 (see Fig. 11). The increased ablation threshold suggests that the energy of the laser pulse is deposited deeper into the graphite surface, producing a stronger thermoelastic response and less heating of the surface.

7.7 The amount of ultrasonic energy generated will depend on the pulse laser energy input (see Fig. 12). Note that all but the lowest energy pulse was ablative in nature. The low amplitude responses from the 0.6 mJ energy level that was primarily thermoelastic may have also been affected by the directivity of the signal, reducing the amount of signal reaching the detector. However, thermoelastic generated waveforms will be consistently lower in amplitude than those generated by ablation. Thermoelastic generation is preferred since it is nondestructive by nature, whereas ablation does alter the surface of the test piece. The reduced amplitude of the thermoelastic waveforms is a detriment to propagation over long distances as illustrated in Fig. 13, but still can be used to perform measurements if the appropriate acoustic wave modes and setups are used (see Fig. 14). Fig. 14 summarizes the results of surface acoustic wave (SAW) velocity measurements for NBG-18 graphite samples subjected to compressive loading. A 4.2 mm focal spot size was used to produce a thermoelastic-generated SAW that propagated 37.1 mm prior to detection. Due to the low signal-to-noise ratio for the low amplitude signals, timing of the peak and trough was used to estimate velocity. The trend of reduced velocity with increased load suggests that mechanical damage was introduced into the graphite proportional to the loading.

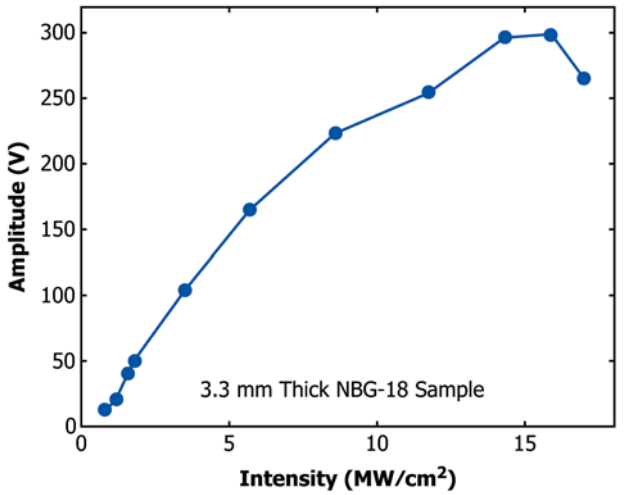

Thermoelastic generation is expected to yield a nearly linear relationship between signal amplitude and laser intensity until energy from the laser pulse is diverted to the ablation process. The downturn in signal amplitude with increasing laser intensity at 14 MW/cm^2 is interpreted to be the ablation threshold.

FIG. 11 Ablation Threshold of NBG-18 Graphite

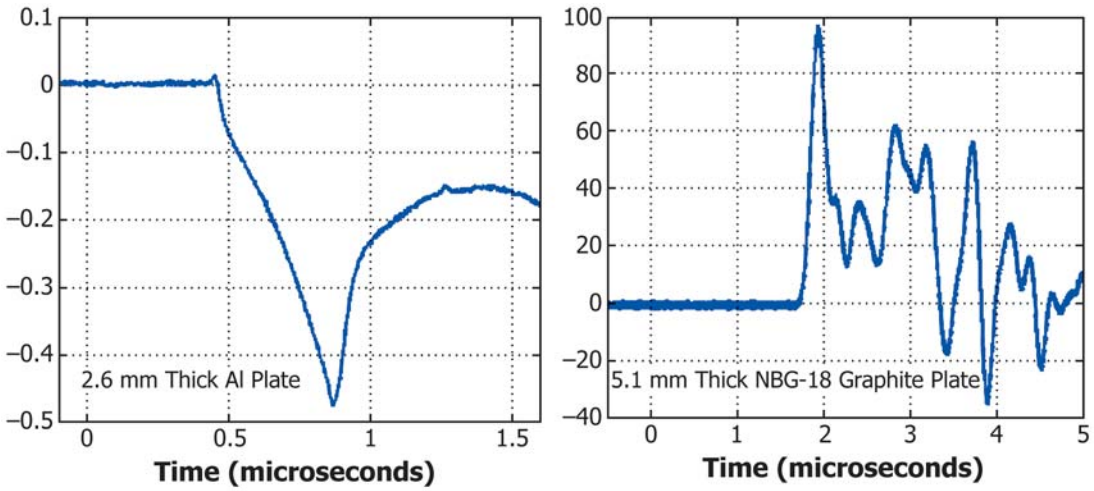

The waveform for the homogeneous aluminum sample is predictable and well defined, while the response from the graphite demonstrates viscoelastic behavior with frequency-dependent dispersion. The graphite response was signaled, averaged, and obtained using a highly ablative source pulse.

FIG. 10 Laser Ultrasonic Responses for Aluminum and Graphite Test Samples

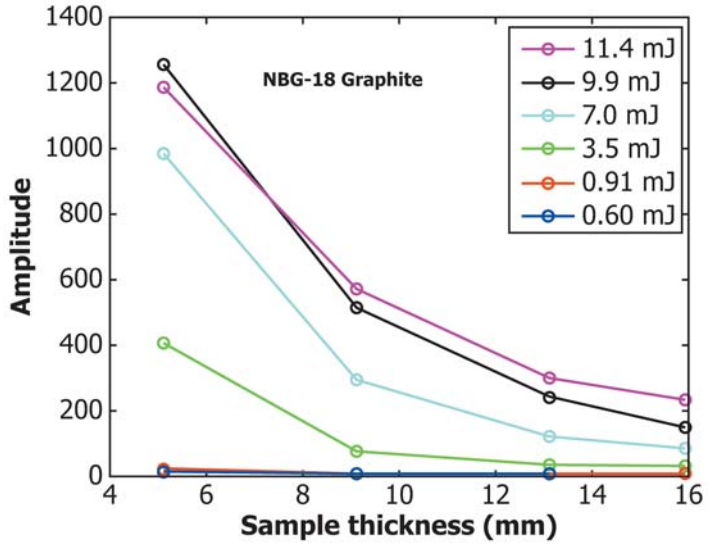

Laser spot size was held constant. Incident energies of 0.91 mJ and above were clearly ablative. At 0.6 mJ, generation was primarily thermoelastic.

FIG. 12 Amplitude of the First Wave Arrival Versus Sample Thickness at Different Pulse Laser Energies

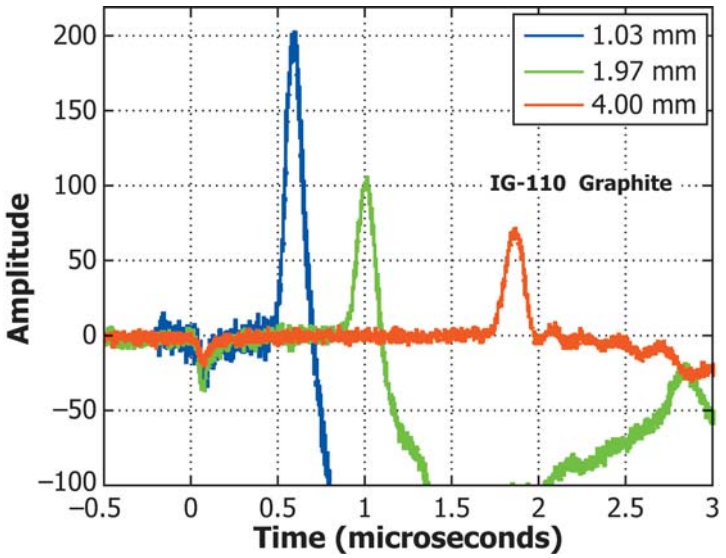

Laser spot size and energy were held constant for each sample. The amplitude of the first wave arrival decreases as thickness increases due to the characteristic attenuation of the graphite structure.

FIG. 13 Thermoelastic-Generated Ultrasonic Waveforms, Recorded from IG-110 Graphite Samples with Thicknesses of 1.03 mm, 1.09 mm, and 4.00 mm

8. X-Ray Examinations

8.1 The use of X-rays for nondestructive examination of materials is based on the partial attenuation of a beam of X-ray radiation as it propagates through a material. X-rays are unaffected, absorbed, or scattered by the material through which they pass. The distribution of unattenuated radiation arriving at a detector provides information about physical properties of the medium. The atomic number of the material and its density are the primary physical factors in X-ray attenuation. The energy of the photons in the X-ray beam is also a factor affecting the attenuation, with higher energy photons less likely to be attenuated. Absorption and scattering interactions may produce subsequent radiation that will either degrade an image or, with appropriate data acquisition protocols, potentially be used to enhance an image or infer additional information.

8.2 *Beer's Law:*

8.2.1 For a monochromatic narrow beam of X-rays passing through a fixed length of homogeneous material (see Fig. 15), the following relationship holds:

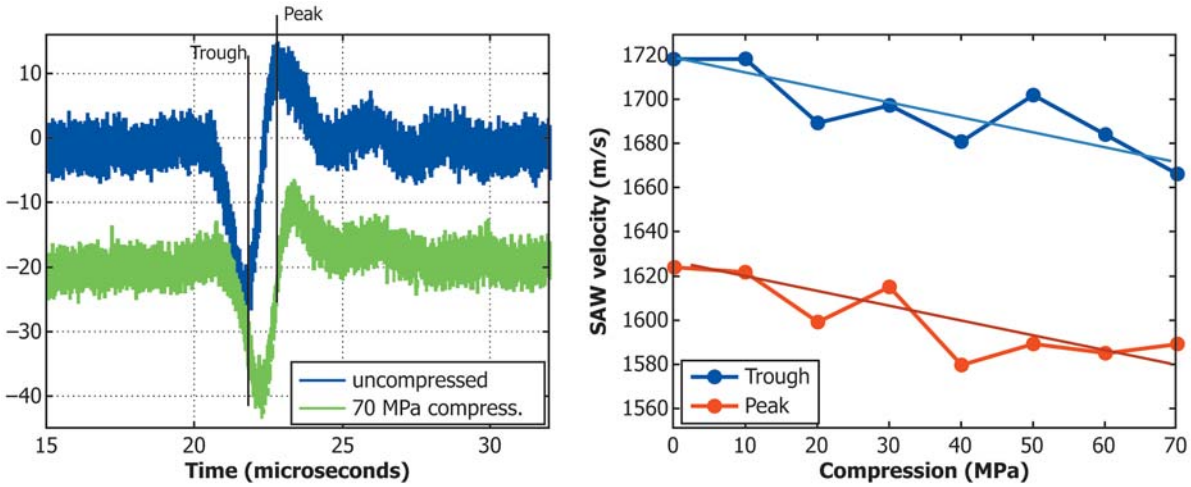

A series of NBG-18 graphite samples were placed under compressive load ranging from 0 MPa to 70 MPa. Subsequent to loading, laser ultrasonics was used to measure the change in surface acoustic wave velocity. Generation spot size was 4.2 mm and the source to detector separation was 37.1 mm. The reduced SAW velocity as the compressive load increases suggests that mechanical damage was introduced into the samples proportional to the loading.

FIG. 14 Surface Acoustic Wave (SAW) Velocity Measurements for NBG-18 Graphite Samples Subjected to Compressive Loading

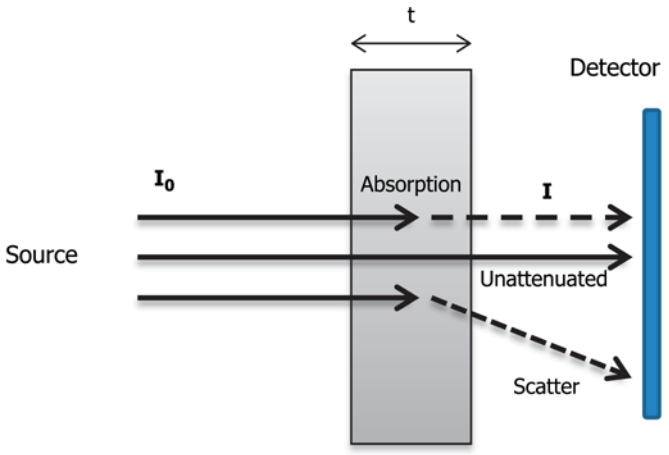

FIG. 15 Beer's Law

$$I = I_o \exp[-\mu t] \tag{3}$$

where:

I_o = the intensity of incoming monochromatic X-ray radiation entering a material,
I = the intensity of the beam of X-rays exiting from a material,
t = thickness of material, and
μ = linear attenuation coefficient of the material.

8.2.2 For a fixed thickness homogeneous material, it is simple to derive the linear attenuation coefficient by taking the log of the equation above:

$$\ln(I / I_o) = \ln(\exp[-\mu t]) \tag{4}$$

$$\mu = -\frac{\ln\left(\frac{I}{I_o}\right)}{t} \tag{5}$$

8.2.3 Beer's law states that the intensity of a beam of radiation drops off exponentially with distance as it passes through a material at a rate subject to the linear attenuation coefficient. More generally, the beam of X-ray radiation may consist of a broad range of energies, the material may be inhomogeneous, the linear attenuation coefficient may vary along the path of the beam, and the material thickness may also vary. Hence the more general relationship is:

$$I(E,r) = I_o(E,r)\exp\left[-\int_o^t (E,Z,r)dx\right] \tag{6}$$

where:

E = the energy of photons in the X-ray beam,
r = position vector locating the X-ray beam, and
Z = the atomic number of the material.

8.2.3.1 Again taking the log of the equation above, we have:

$$\ln\left(\frac{I}{I_o}\right) = -\int_o^t \mu(E,Z,r)dx \tag{7}$$

8.2.4 When a transmission X-ray image is acquired, the information recorded represents the equation above and after processing; at each point in the image, the result is dependent on a sum of the linear attenuation coefficients through the material. Hence a 2D radiograph represents the summation or collapse of spatial information (that is, linear attenuation coefficient) along the direction that the interrogation radiation passes. It is possible to unfold this summation and achieve a pointwise representation of the linear attenuation coefficient through the application of computed tomography techniques.

8.2.5 Graphite is an inhomogeneous material comprised primarily of a single element, carbon. Based on the method of manufacture, variations may occur in density throughout the material and may range from minor density variations to substantial porosity. Transmission X-ray imaging may be employed to characterize the variations in density of graphite by deriving the density-dependent linear attenuation coefficient. From an imaging perspective, we may consider graphite to be a single element with Z = 6 and an average bulk density in the range of 1.7 g⁄cc to 1.9 g⁄cc. To obtain spatially dependent estimates of density, either 2D transmission radiography or 2D or 3D transmission computed tomography may be

used. Transmission-computed tomography is preferred as it allows for a pointwise map of density/porosity throughout the object/region of interest. To optimally use X-ray transmission techniques, one has to select appropriate hardware including a source of X-rays, X-ray detector, and, if using scanning techniques or computed tomography, appropriate motor-driven stages to move either the object, the source-detector pair, or some other combination of these components. The object attributes that impact the selection of hardware include the overall dimensions, the thickness variations, the density, and composition. Attributes that are desired in the resultant image also impact the selection of hardware, the image acquisition protocol, and the processing of the image. The primary image attributes of interest are spatial resolution and image contrast.

8.2.6 The image should faithfully represent the property of interest at each point in either the 2D or 3D result. Two extremes in the imaging process need to be avoided. If there is any path of radiation through the object that is either 100 % attenuated by the object, or if radiation passes through the object completely unattenuated, the resulting image will not provide any useful information for the object along this path. Hence it is necessary to select the X-ray source and the dimensions of the object (if possible) such that both of these extremes are avoided. It may not be possible to choose the size of the object under inspection, so a source of X-rays needs to be chosen such that some fraction of the beam intensity is attenuated through each path. X-ray imaging requirements scale in an obvious way; smaller and lower density objects require lower energy sources of X-rays, while thicker and higher density objects require higher energy sources of X-rays to accomplish the desired penetration through the object. Spatial resolution in the final image may be partially dependent upon the spatial extent of the source (or spot size) when magnification is employed. If an object has appreciable thickness, the magnification of features in the object from the source side to the detector side decreases. Hence, spatial resolution may be poorer for features residing closer to the source, even if the object is placed directly in front of the detector. Lower energy sources are capable of having smaller spot sizes and hence offer the potential of higher spatial resolution. Hence one tradeoff that must be considered is the sacrifice of spatial resolution in order to enable sufficient penetration (by means of higher energy) through the object.

8.2.7 There are several points to consider for X-ray inspection of graphite, including:

8.2.7.1 Adequate penetration of a variable thickness, variable porosity material for good contrast (range of intensity values) with a broadband (Bremsstrahlung) source.

8.2.7.2 Contrast resolution of the imaging system.

8.2.7.3 Spatial resolution of the imaging system.

8.2.7.4 Image acquisition protocols: digital radiography, two-dimensional computed tomography, three-dimensional computed tomography.

8.2.7.5 Image processing to derive spatially dependent density/porosity estimates.

8.2.8 Fig. 16 shows the energy dependent linear attenuation coefficient for carbon for an assumed density of 1.7 g⁄cc. The graph is derived from information provided by the National Institute of Standards and Technology.[4] This total attenuation coefficient represents a summation of independent attenuation coefficients based on several types of absorption and scatter mechanisms. Note that the curve is nearly linear on a log-log plot with two distinct linear components diverging around 30 keV.

8.3 *Penetration to Support Detection:*

8.3.1 Fig. 17 uses the information from Fig. 16 to derive a transmission ratio (I/I_o) for several thicknesses of homogeneous carbon at 1.7 g⁄cc. This graph may be used to determine an appropriate range of X-ray energies for inspection of graphite material. It is useful to consider an energy range because the most common type of X-ray source used is a

[4] Available at: http://www.nist.gov/pml/x-ray-mass-attenuation-coefficients.

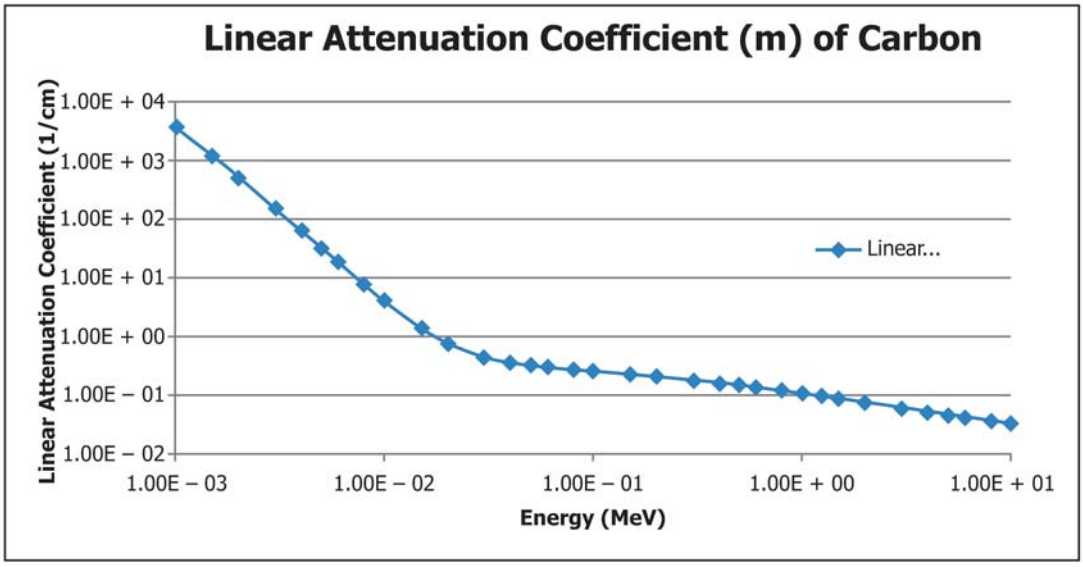

FIG. 16 Linear Attenuation Coefficient of Carbon

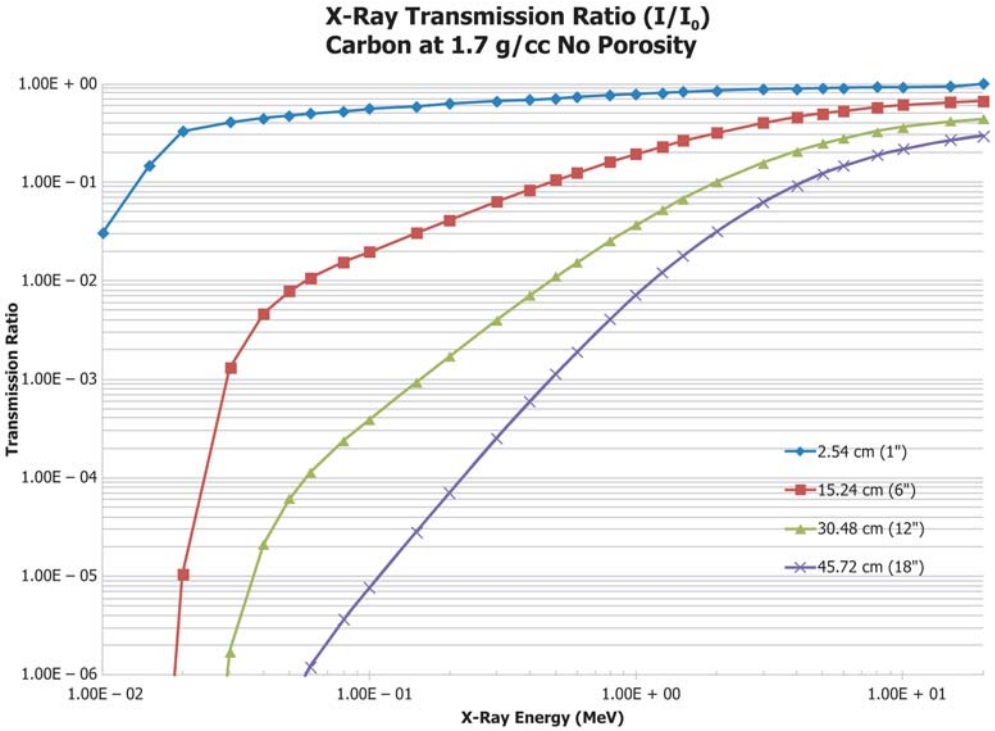

FIG. 17 X-Ray Transmission Ratio for Several Thicknesses of Carbon

generator source which produces a very broad X-ray energy range. Other types of sources (isotopic or synchrotron) can produce monochromatic or very narrow band energies but are more special purpose and less common. Suppose a graphite object varies in thickness from 15.24 cm to 30.48 cm. If we require a minimum transmission ratio of 1.0 % (1.0e-02), then the minimum X-ray energy needed for the 30.48 cm thickness is roughly 500 keV. This energy yields a 10 % transmission ratio for the 15.24 cm thickness and only 0.1 % for the 45.72 cm thickness. If we also limit the maximum transmission ratio to about 50 % (5.0e-01), then for the 15.24 cm thickness we would require an X-ray energy no greater than about 5.0 MeV. At that energy, the transmission ratio for the 30.48 cm thickness is about 25 %. Thus the range of transmission ratios would be 10 % to 50 % at 15.24 cm and 1 % to 25 % at 30.48 cm for an energy range of 500 keV to 5.0 MeV.

8.3.2 It is more often the case that there would be a limited number of options in choosing a source. For example, a radiography facility may have access to only one or two X-ray generators. So a more practical approach for determining whether there will be sufficient penetration would be to consider the range of energies provided by the source to obtain transmission ratios. For example, consider a 450 kVp X-ray generator that produces a broad spectrum of energies whose maximum energy is 450 keV but has a peak of energy output in the range of about 200 keV to 300 keV. For the 30.48 cm thickness of carbon, the intensity ratio runs from about 0.17 % (at 200 keV) to 0.4 % (at 300 keV). In this case, the 450 kVp source may be insufficient in energy to provide an adequate intensity range of unattenuated radiation to properly expose the detector.

8.4 *Detector Dynamic Range to Support Image Contrast:*

8.4.1 Subject contrast is defined (Guide E94) as the ratio of radiation intensities transmitted by two selected portions of a specimen. Given that a source of X-rays is used that provides a range of intensity ratios for a range of object conditions (thickness and density/porosity variations), the detector must be able to adequately record and preserve the intensity variations. Similar to the considerations of too much or too little radiation passing through the object, we must also avoid the cases of detector saturation (too much radiation) or underexposure (radiation that creates a signal lower than the detector noise). Those conditions lead to a total loss of information.

8.4.2 Electronic imaging X-ray detectors now routinely offer 12 bit to 20 bit digitization ranges. There is typically some loss of dynamic range during the analog-to-digital process due to noise occurring over several conversion processes (X-ray to visible light, visible light to electronic signal, pre-amplification, digitization) such that the X-ray detection process can provide a true dynamic range from 10 bits to 18 bits or 1024 to 262, 144 discrete intensity levels. For the conversion of X-ray to visible light, efficiency is highest for scintillator materials that can be manufactured to design thicknesses optimized for the energy range of X-rays. These are typically solid-state crystals composed of cadmium tungstate and are most often used in linear detector arrays. Alternatively, lower efficiency phosphors such as gadolinium oxysulfide and cesium iodide are often used in area detector arrays, however conversion efficiency drops off dramatically at higher X-ray energies.

8.5 *Spatial Resolution:*

8.5.1 Spatial resolution refers to the ability of the imaging system to preserve dimensional features of the object under inspection. Chapter 13 of the ASNT Radiographic Testing

Handbook defines spatial resolution as the size of the smallest detectable feature in the object (**5**). A system analysis incorporating source spot size, geometric magnification, detector spatial resolution, post processing, and image discretization may be performed to derive an expected spatial resolution. There are also several experimental methods defined to measure spatial resolution, including the use of image quality indicators (Practice E1025) and measurement of the modulation transfer function (Guide E1441). Spatial resolution scaling occurs as systems go from very small to very large to assess very small to very large objects. Micron size pores will only be preserved in an image when the object is very small and the imaging system employs either high magnification, extremely high detector spatial resolution, or some combination of these, and potentially advanced scanning techniques. As systems become larger and use higher energies to accommodate larger, denser objects, spatial resolution increases in size (that is, becomes comparatively poorer). Hence in larger systems, microporosity is not measurable or even observable though it may contribute to an apparent lower average density per volume element in an image. The spatial resolution of the imaging system will limit the minimum size of pore that may be observed and measured in the object.

8.6 *Image Acquisition Protocol and Data Processing:*

8.6.1 Options for image acquisition include two-dimensional projection radiography (film or electronic), two-dimensional computed tomography producing one or more slices through an object and potentially building a three-dimensional image from multiple slices, and three-dimensional computed tomography. Choosing between radiography and computed tomography determines whether information obtained represents a pointwise density/porosity estimate (from tomography) or an estimate of the summation of density/porosity along a path of radiation.

8.6.2 A wide variety of image processing techniques is available for attempting to enhance spatial and contrast resolution, deriving and quantifying features of interest (estimates of local porosity for example), and for image presentation. The ASNT Radiographic Testing Handbook, Chapter 13, describes many of these techniques (**5**). Kane et al. have provided a specific demonstration of microstructural characterization of graphite (**6**).

8.7 *Examples:*

8.7.1 Fig. 18 shows a projection radiograph of a graphite block (~50 mm by 152 mm by 400 mm) acquired with a vertically scanning linear diode detector array. The image was obtained with an X-ray generator set to 200 kVp, 2.3 mA. The spatial resolution of the imaging system is roughly 1 mm. The exposure time for each line in the image is 0.4 s. Several large porous regions (black in the image) can be observed. Also seen are some bright (white) spots that indicate high density materials that have contaminated the graphite. There also appears to be a minor and slowly varying density change throughout the object as seen by slow spatial variations of gray.

8.7.2 Fig. 19 shows tomographic slices of a graphite cylinder with holes drilled to demonstrate spatial resolution. The top image shows the image acquisition system that may be used to acquire either 2D projection radiographs by means of vertical scanning or 2D computed tomography slices by means of object rotation. The holes are 1 mm, 2 mm, 4 mm, 6 mm, and 8 mm diameter. The image was obtained with an X-ray generator set to 220 kVp, 2.3 mA. The two circular images in Fig. 19 are horizontal slices from different vertical positions in the cylinder that show the drilled holes and some areas of porosity (on the right image). The lower right rectangular image is a vertical slice showing the 1 mm drilled hole and a broken drill bit at the bottom of the hole.

8.7.3 Fig. 20 shows tomographic slices of three different sizes of graphite samples, scanned with three different X-ray inspection systems. It demonstrates the scalability of X-ray inspection techniques. The 5 mm diameter sample was scanned using a microfocal X-ray source at 40 kVp using 3D cone beam tomography. This system is capable of providing spatial resolution of a few microns. The 152 mm sample was scanned with a linear diode detector array using 2D tomography. This system is capable of 1 mm spatial resolution. The 483 mm sample was also scanned using 2D tomography. Spatial resolution is approximately 2 mm for this image.

9. Keywords

9.1 carbon; eddy currents; graphite; inspection; nondestructive evaluation; ultrasonics; X-ray radiography

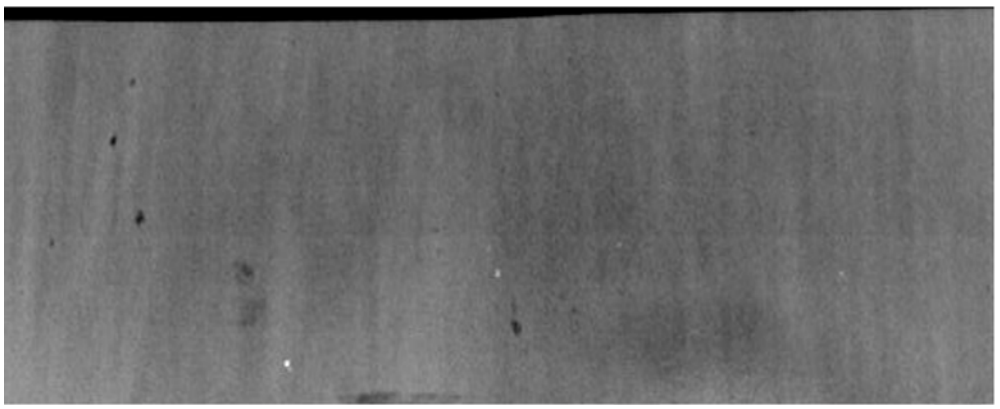

FIG. 18 2D Projection Radiograph of a 50 mm Thick Graphite Block

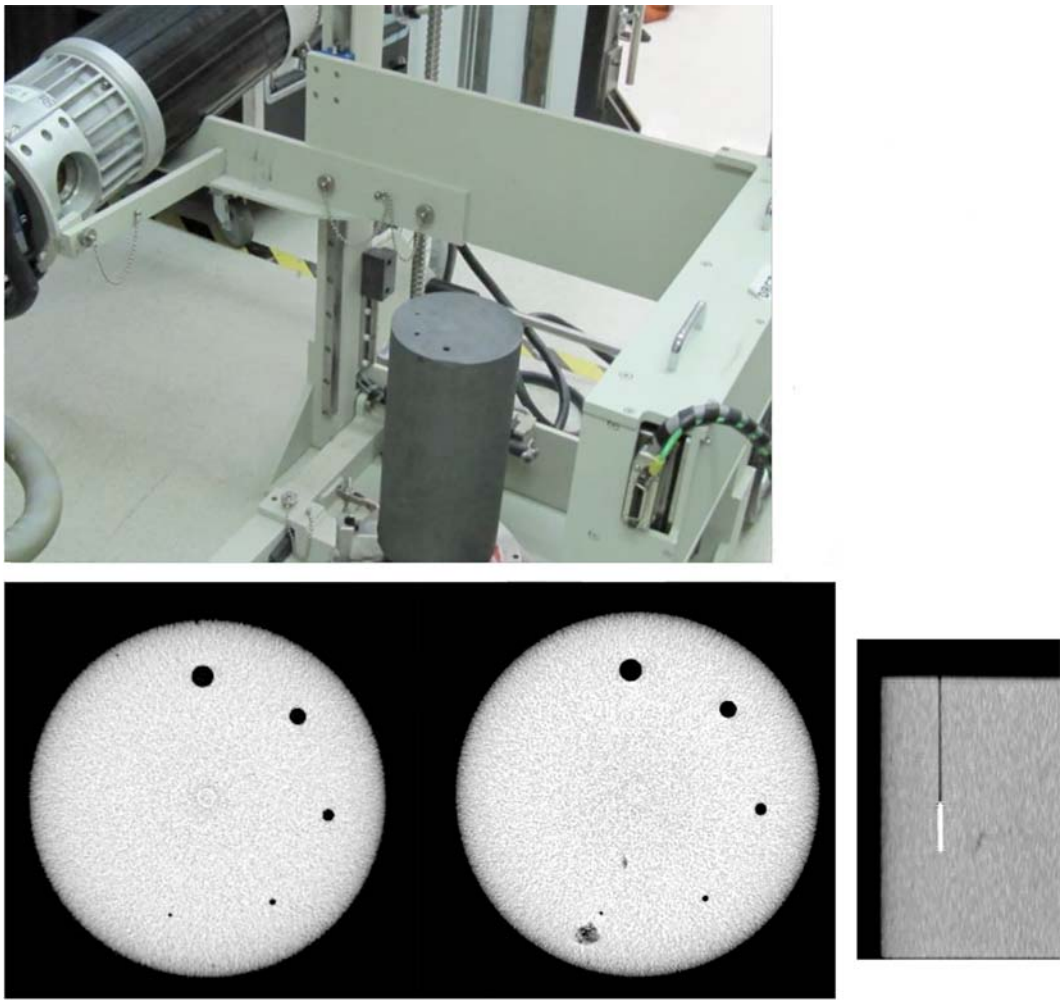

FIG. 19 Graphite Cylinder Scanned with Linear Diode Array and Tomographic Images

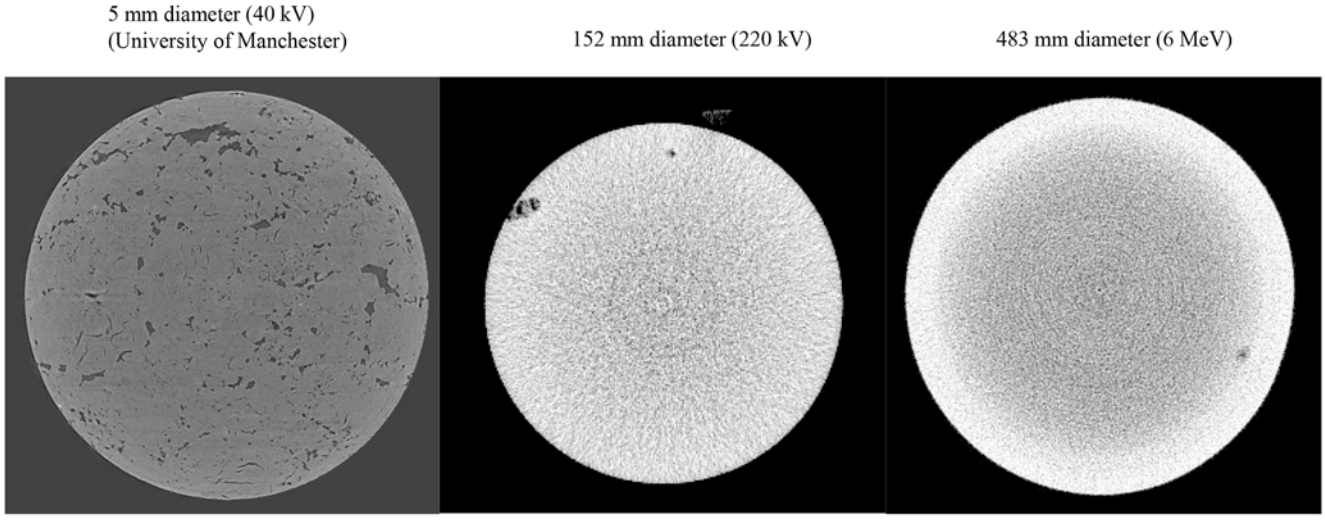

FIG. 20 Tomographic Images of Graphite Samples of Different Sizes

REFERENCES

(1) *Nondestructive Testing Handbook, Second Edition, Volume Four: Electromagnetic Testing*, American Society for Nondestructive Testing, Columbus, OH, 1986, p. 664.

(2) Hagemaier, D. J., *Fundamentals of Eddy Current Testing*, American Society for Nondestructive Testing, Columbus, OH, 2005.

(3) Dutton, B., and Dewhurst, R. J., "Graphite Anisotropy Measurements Using Laser-Generated Ultrasound," *Journal of Optics A: Pure and Applied Optics*, Vol 9, 2007, pp. S7–S11.

(4) Schmerr Jr., L. W., *Fundamentals of Ultrasonic Nondestructive Evaluation: A Modeling Approach*, Springer, New York, NY, 1998.

(5) *Nondestructive Testing Handbook, Third Edition, Volume Four: Radiographic Testing*, American Society for Nondestructive Testing, Columbus, OH, 2002.

(6) Kane, J., Karthik, C., Butt, D. P., Windes, W. E., and Ubic, R., "Microstructural Characterization and Pore Structure Analysis of Nuclear Graphite," *Journal of Nuclear Materials*, Vol 415, 2011, pp. 189–197.

RELATED MATERIAL

ASTM Practice E746 for Determining Relative Image Quality Response of Industrial Radiographic Imaging Systems

ASTM Guide E1000 for Radioscopy

ASTM Practice E1255 for Radioscopy

ASTM Terminology E1316 for Nondestructive Examinations

ASTM Practice E1570 for Computed Tomographic (CT) Examination

ASTM Practice E1647 for Determining Contrast Sensitivity in Radiology

ASTM Guide E1672 for Computed Tomography (CT) System Selection

ASTM Test Method E1695 for Measurement of Computed Tomography (CT) System Performance

ASTM Practice E1742/E1742M for Radiographic Examination

ASTM Practice E2002 for Determining Total Image Unsharpness and Basic Spatial Resolution in Radiography and Radioscopy

ASTM Guide E2007 for Computed Radiography

Practice E2033 for Computed Radiology (Photostimulable Luminescence Method)

ASTM Practice E2698 for Radiological Examination Using Digital Detector Arrays

ASTM Guide E2736 for Digital Detector Array Radiology